

Iapetus surface variability revealed from statistical clustering of a VIMS mosaic

Noemi Pinilla-Alonso¹ and Giuseppe A. Marzo²

¹ NASA Postdoc. Program - ORAU, NASA Ames Research Center, Moffett Field, CA, USA

² ENEA, C.R. Casaccia, UTFISST-RADSITO, Roma, Italy

Abstract

We present the study of a collection of spectra of Iapetus obtained with VIMS, the Visual and Infrared Mapping Spectrometer on board of Cassini spacecraft. The data evaluated ($\sim 1.3 \times 10^4$ spectra from 0.35 to 5.1 μm) were obtained during the second flyby of Iapetus, in September 2007. We apply statistical clustering to address the surface composition of Iapetus. We identify 7 statistically distinct units on Iapetus' surface and compare the main characteristics of their representative spectra (centroids).

1 Introduction

Saturn's third largest satellite, Iapetus (radius 720 km), occupies a near-circular orbit locked in synchronous rotation such that it keeps one hemisphere permanently directed toward Saturn throughout its 80 day orbital period. From approximately the time of its discovery [3], it has been known to have the unique property among planetary satellites that its leading hemisphere (the one that faces forward in its orbit around Saturn) has a very low surface reflectance (geometric albedo) of about 2%–6%, while the trailing hemisphere of the satellite is 10 times more reflective. The dark material extends toward the trailing side near the equator, and the bright trailing-side terrain extends over the poles even on the dark side. The composition of the low-albedo material, its origin, and the peculiarity of its geographic distribution have all made Iapetus an object of special interest not only in Saturn's family of satellites but in the entire solar system. The recent discovery by [23] of a large dark ring circling Saturn within, and co-rotating with the orbit of Phoebe, has given a strong support for the theories that suggest Phoebe could be the source of the low-albedo material on the surface of Iapetus [21]. [22] present a global thermal model of the distribution of the dark and bright material on Iapetus, in this model, the exogenous dark material is suggested to be dust swept up by the leading hemisphere of Iapetus' surface as it leaks and migrates toward Saturn from the large dust ring originating from Phoebe [23]. According to [22] the

inflow of exogenous material would raise the local temperature triggering a runaway thermal imbalance and migration of volatiles as water ice to the cooler regions of the satellite (i.e., trailing hemisphere and poles). Native dark dust entrained in the icy crust of Iapetus also contributes to the low-albedo layer as a lag deposit, resulting from the thermal mobility of H₂O ice over long time scales.

The Cassini spacecraft entered the Saturn system in 2004 with the aim of providing a closer insight on the planet, its satellites and rings to broaden our knowledge about this complex system. VIMS, the Visual and Infrared Mapping Spectrometer, was designed to collect spectra for spatially resolved areas on the surface of the target [1]. Since June 2004 Cassini spacecraft has performed numerous flybys of the icy satellites collecting a voluminous amount of data with a wide range of distances from the moons and illumination geometries. In 2007 it approached Iapetus at a minimum distance of 1620 km providing the highest spatial resolution data during Cassini's primary mission.

Here we present the results of some of the work on a selection of Iapetus VIMS observations, including: selection of the data (Section 2.1), mosaicking (Section 2.2), clustering (Section 3) and preliminar spectral analysis (Section 4).

2 Data

2.1 VIMS data

VIMS consists of two imaging spectrometers operating in the VIS (0.35–1.05 μm) and the IR (0.88–5.10 μm) ranges [1]. The VIS channel has 96 wavelengths, a spectral resolution of 0.0073 μm , and spatial resolutions of 0.50 (nominal) or 0.166 (high-resolution) mrad/pixel. The IR channel has 256 wavelengths, a spectral resolution 0.0016 μm , and spatial resolutions of 0.50 (nominal) or 0.25×0.50 (high-resolution) mrad/pixel. The typical VIMS observation produces what is commonly called a hyperspectral cube or cube for short, consisting of 64×64 pixels in the spatial dimensions and 352 pixels in the spectral dimension.

Our sample consists of a selection of data obtained by VIMS during the Iapetus fly-by on September 10th, 2007. On Cassini orbit 49, 80 cubes of data were obtained during part of sequence 33. Among these we selected 30 cubes that were taken in nominal resolution mode, i.e. both spectrometers are operated at the same spatial resolution (IFOV 0.5×0.5 mrad/pixel) and approximately cover the same region, and where both VIS and NIR spectra showed good quality (neither too noisy nor saturated).

2.2 Mosaicking

The spectra analyzed as part of this work were calibrated to I/F using the VIMS pipeline with the RC17 calibration [4, 17, 8]. These selected cubes were despiked to avoid single-spectral channel deviations. A global set of 25968 spectra, covering the full range between 0.35 and 5.1 μm , has been considered for integration into the mosaic.

The next step was the geometric map projection (georeferencing, hereafter), which re-

quires geometric calibration information of the instruments for each pixel, position of the Cassini spacecraft, and pointing data of each observation frame that are provided by SPICE kernels that are available from the PDS. VIMS observations in different spectral ranges all differ in spatial resolution and observe slightly different fields of view [12]. We georeferenced the two spectral ranges (i.e., VIMS VIS and IR) separately since specific geometric information is available for each. After georeferencing, the pixels of the two spectral ranges co-register but still differ in size. As demonstrated by [12] and [18], geometric co-registration strongly improves the spectral co-registration resulting in a smooth transition of the spectral signal across distinct spectral ranges (cf., Fig. 2 from [12]).

Finally, each observation was spatially oversampled to the finest surface resolution available for the sample. To accomplish this the individual observations have been sorted by pixel ground resolution, and the image cube with the highest resolution has been placed on top of the mosaic. The selected spatial resolution of the mosaic is therefore defined by the image data cube with the highest spatial resolution of the set that is $0.5^\circ/\text{pixel}$ in our case.

The final mosaic, Fig. 1 a,b, covers a wide range of Latitude ($47^\circ\text{ S} - 27^\circ\text{ N}$) and Longitude ($142^\circ - 235^\circ\text{ West}$). The area observed includes part of the leading and trailing hemispheres and the boundary between them assuring good coverage of units with different compositions. After eliminating redundant information that comes from the areas covered by different cubes, the mosaic is composed of 12981 spectra (see Fig. 1 b).

3 Clustering

3.1 Clustering technique

We use a statistical data technique to produce clusters of spectra having similar properties [14, 15, 16]. The cluster averages, or centroids, and their associated variability produce a significant reduction of the original data volume but retain the quantitative properties of the original data set. Our cluster analysis technique has been extensively validated against spectral data sets and applied to different objects of the solar system [14, 15, 16, 18, 19, 10]. It consists of a K-Means cluster algorithm [13, 11] and we adopt the criterion of [2] to prevent sub-optimal solutions and test for the influence of the random noise of the measurements. The final cluster configuration is independent of the random noise, while remaining sensitive to systematic errors such as instrumental effects. The clustering technique is agnostic about the meaning of the clusters and scientific interpretation requires subsequent evaluation of the clusters.

3.2 Cluster analysis

Before applying the cluster analysis to our sample all the spectra were normalized to 1.0 at $1.2\ \mu\text{m}$ to minimize the effect of the albedo in the results. We found 10 clusters but for subsequent analysis we select 7 of them that cover more than 99.6% of the mosaic. The other three clusters were discarded because they contain spectra showing some saturated or noisy pixels.

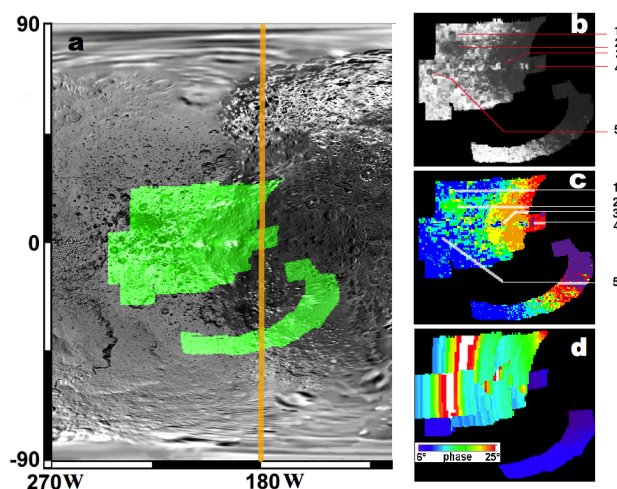


Figure 1: (a). Area covered by the mosaic overlapping map of Iapetus (NASA/JPL/Space Science Institute). The orange line at 180° W, represents the limit between the leading (on the right) and the trailing (on the left) hemisphere. The mosaic covers part of the CASSINI REGIO (dark side of Iapetus) and part of the icy trailing (bright side of Iapetus) hemisphere with some dark craters. Some mountains are visible on the equator over the ridge as bright spots around 200° W. (b) Mosaic seen at $1.738 \mu\text{m}$. This mosaic contains 12981 pixels, each of them covering 0.5° ; (c) Selected clusters. Each color shows the pixels that belong to the same cluster. All the pixels in the same cluster will be represented by the same average. Labels on panels (a) and (b) show some geographical formations [1. Baligant crater; 2. Dark area no named yet by the IAU; 3. Cordova Montes; 4. Sorence and Haltile Montes; 5. Garlon crater]; (d) Phase Angle values over the mosaic, extracted from the backplanes. It varies from 6 to 25° .

The distribution of the spectral clusters in the mosaic is shown in Fig. 1 c. They exhibit a spatially coherent distribution when compared with the detailed geomorphology and albedo dichotomy of Iapetus (Fig. 1 a,b) suggesting that the slightly different illumination geometry of the VIMS observations forming the mosaic do not significantly affects the clustering results.

4 Analysis of the centroids

To evaluate if the clusters are representative of different surface compositions we need to study the spectral information conveyed by their centroids. Different levels of brightness are indicated by the value of I/F continuum. In Table 1 we show the values of I/F for each centroid at $1.2 \mu\text{m}$ before normalization. The darkest areas on the surface correspond to the purple cluster and the brightest are represented by the blue one.

Spectral slopes (S) allow to measure colors of the surfaces of icy objects. We computed

Table 1: $I/F_{1.2\mu\text{m}}$ and S for selected centroids (see Sect. 4 for definitions)

Centroid	$I/F_{1.2\mu\text{m}}$	S
Blue	0.32	0.13
Cyan	0.21	0.15
Green	0.13	0.23
Yellow	0.10	0.33
Orange	0.09	0.34
Red	0.07	0.42
Purple	0.05	0.48

$S[\mu\text{m}^{-1}]$ by the best linear fit to the I/F normalized as explained in Section 3.2, between 0.7 and 1.4 μm where the centroids are featureless: $S = \frac{(I/F)_{1.4} - (I/F)_{0.7}}{0.7 \times (I/F)_{1.2}}$. Neutral slopes ($S \sim 0$) in this range are typical of surfaces rich in water ice; yellow and red ($S > 0$) are typical from silicates and organic compounds that can be part of the dark material or contaminants in the ice.

As expected based on previous studies of the surface of Iapetus ([9], and references therein), the centroids (see Fig. 2) show features of water ice (1.5, 2.0 and 3.0 μm), CO_2 (4.26 μm), OH-bearing materials (broad band ~ 3.0), complex organic materials (3.29 μm), and possibly other components (0.35 to 0.7 μm hump and 2.4 μm), not definitely identified, as suggested by [9] and references therein.

4.1 Blue and Cyan clusters: water ice rich surface

These clusters are represented by two centroids that are neutral in the visible and exhibit strong spectral bands at 1.5, 2.0 and 3.0 μm that are consistent with the presence of H_2O ice. The 3 μm band appears saturated suggesting that water ice must be dominant on this surface and/or the ice must form an optically thick layer. The strong decrease of the reflected light between 2.2 and 2.6 μm and beyond 3.6 μm can be due to water ice.

Variations in phase angle might be responsible for changes in depth of the H_2O ice features. However comparing Fig. 1c with the phase angle map of the same mosaic, Fig. 1d, it is evident that the clusters are not correlated with the illumination geometry. For example, the lower right portion of the mosaic in Fig. 1d shows that phase angle is mostly constant throughout this region of interest while Fig. 1c shows the entire range of clusters. Additionally, in the upper left part of Fig. 1d a wide range of phase angles are encountered and the blue cluster in Fig. 1c extends across much of this area.

The band at ~ 4.25 μm is subdued in the blue unit while it is more evident in the cyan one. There is a shift of this band with respect to the center of the absorption of pure CO_2 ice that is nominally centered at 4.268 μm . The origin of this shift is studied in detail in the spectra of several Saturn's Satellites [6]. These shifts from the nominal laboratory values for pure CO_2 occurs when this volatile appears as a molecular mixture with other molecules or

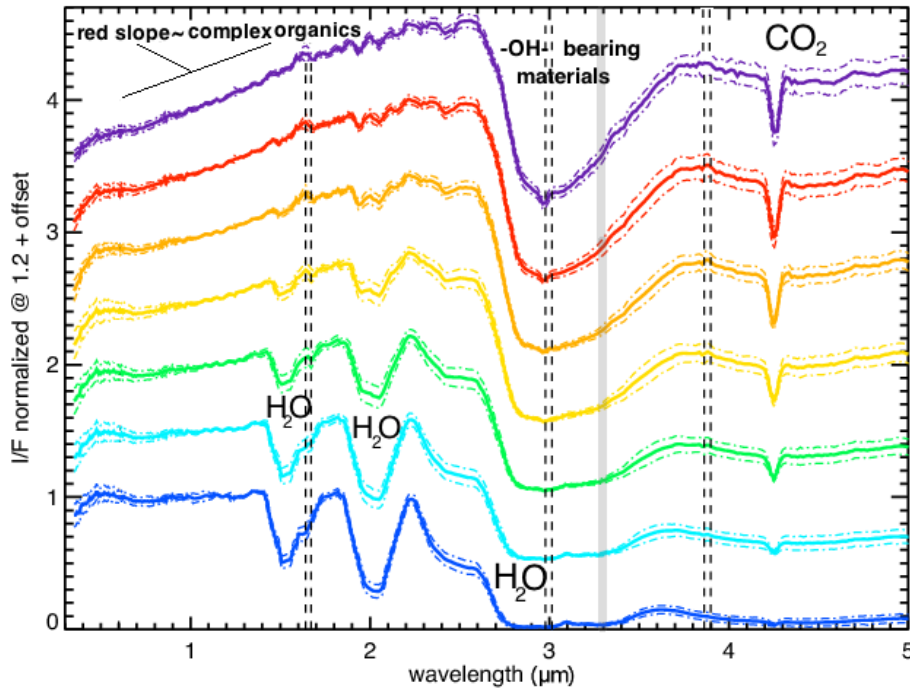


Figure 2: Centroids (continuous colored lines) and standard deviation (dash-dot colored lines) of each cluster. The colors are chosen following the colors of the clusters in Fig. 1 b. Main features of the spectra are labeled. The grey thick vertical line indicate where PAH and aliphatic bands have been detected on Iapetus dark material [5]. Blue and Cyan clusters, the ones that overlap the brightest parts of the mosaic (Table 1), are characterized by water ice absorptions. On the other extreme, red and purple centroids, show signs of complex organic material. The other three clusters show signs of both of these compounds. The dashed vertical lines indicate bad pixels due to the junction of the VIMS-IR order-sorting filters.

when CO_2 appears in clathrates.

4.2 Purple and Red clusters: complex organic rich surface

These clusters are represented by the two reddest centroids in our sample (see slopes in Table 1) that spatially correlate with the darkest surface of the mosaic (see I/F values in Table 1). These red slopes in the visible spectra of icy objects are traditionally associated with the presence of complex organics that are formed as irradiation products of simple hydrocarbons [20]. In the absence of clear diagnostic spectral features in most of them, the composition of this dark material is generally inferred to be carbon-rich, but the exact form(s) of the carbon is unknown.

Furthermore, detection of aromatic and aliphatic hydrocarbons on Iapetus and Phoebe [5] show the presence of these hydrocarbons in the low-albedo material of these satellites.

The distribution of these materials on the surface of Iapetus has been studied using the same mosaic as in [7]. The CO₂ ice band at $\sim 4.25 \mu\text{m}$ is prominent in the spectra of these clusters (Fig. 2).

4.3 Orange, Yellow and Green clusters: boundary regions

The spectra of these clusters have characteristics of the four previous groups. They exhibit a moderate red slope in the visible and weaker bands of water ice. One hypothesis is that the dark and bright material is mixed in the regions delimited by these clusters, support for this hypothesis comes from the fact that these clusters overlay the boundaries between the dark and bright material, where more mixing is expected. CO₂ ice band at $\sim 4.25 \mu\text{m}$ is present in these clusters (Fig. 2).

5 Conclusions

- By using cluster analysis we focus the study of $\sim 1.3 \times 10^4$ spectra to the study of 7 that represent the 99.6% of the selected sample.
- We find coherence between the distribution of the clusters and geographical features on the surface.
- Phase angle and albedo are not first order factors affecting the result of the clustering.
- The characteristics of the 7 centroids suggest a different composition based on: 1) differences in the brightness of the surface (I/F values); 2) differences in the slope in the visible that could be related to the presence of complex organics; and 3) differences in the shape of the bands and in the bands identified.
- Carbon dioxide appears widespread over all the surface of the mosaic.

More detailed analysis of these reflectances are needed to shed light in the knowledge of the nature of bright and dark material on Iapetu's surface.

Acknowledgments

The authors of this paper want to acknowledge the continuous and valuable support received from Ted. L. Roush, Dale. P. Cruikshank and Cristina Dalle-Ore, this work benefited from discussion with them. NPA wants to acknowledge the support from NASA Postdoctoral Program administered by Oak Ridge Associated Universities through a contract with NASA. GAM acknowledges NASA's Planetary Geology & Geophysics program for supporting part of this research.

References

- [1] Brown, R. H., et al. 2004, Space Sci. Rev. 115 (1-4), 111

- [2] Calinski & Harabasz 1974, *Communications in Statistics*, 3, 1
- [3] Cassini, G. D. 1672, *Phil. Trans.* 12, 831; quoted in Alexander, A.F.O.D., 1962. *The Planet Saturn*. McMillan, New York, 474 pp.
- [4] Coradini, A., Filacchione, G., Capaccioni, F., et al., 2004, *P&SS*, 52, 661
- [5] Cruikshank, D. P., Wegryn, E., Dalle Ore, C. M., et al. 2008, *Icarus*, 193, 334.
- [6] Cruikshank, D. P., Meyer, A. W., Brown, R. H., et al. 2010, *Icarus* 206, 561
- [7] Dalle Ore, C. M., Pinilla-Alonso, N., Marzo, G. A., et al. 2010. P5.4. Symposium "PAH and the Universe" (pdf file in <http://pahconf.cesr.fr/pdf/12-updatedBooklet-sympPAH.pdf>).
- [8] Filacchione, G., Capaccioni, F., McCord, et al. 2007. *Icarus*, 186, 259
- [9] Filacchione, G., Capaccioni, F., Clark, R. N., et al. 2010, *Icarus*, 206, 507
- [10] Fonti, S., & Marzo, G. A. 2010, *A&A*, 512, 51
- [11] Hartigan, J. A., & Wong, M.A. 1979, *Journal of the Royal Statistical Society*, 28, 100
- [12] Jaumann, R., Stephan, K., Brown, R.H., et al. 2006, *P&SS* 54, 1146
- [13] MacQueen, J. B. 1967, *Proceedings of 5th Berkeley Symposium on Mathematical Statistics and Probability*, 281
- [14] Marzo, G. A., Roush, T. L., Blanco, A., et al. 2006, *JGRE*, 111, CiteID E03002.
- [15] Marzo, G. A., Roush, T. L., Blanco, A., et al. 2008, *JGRE*, 113, CiteID E12009.
- [16] Marzo, G. A., Roush, T. L., & Hogan, R. C. 2009, *JGRE*, 114, CiteID E08001.
- [17] McCord, T. B., Coradini, A., Hibbitts, C. A., et al. 2004, *Icarus*, 172, 104
- [18] Pinilla-Alonso, N., Roush, T. L., Marzo, G., et al. 2009, *AGUFM2009*, P51C-1144.
- [19] Pinilla-Alonso, N., Marzo, G., & Cruikshank, D. P., 2009, *AGUFM2009*, P21B-1214
- [20] Sagan, C. & Khare, B. N. 1979, *Nature*, 277, 102
- [21] Soter, S. 1974, *IAU Colloquium 28*, Cornell University
- [22] Spencer, J. R., & Denk, T. 2010, *Science*, 327,432
- [23] Verbiscer, A., Skrutskie, M., & Hamilton, D. P. 2009, *Nature* 461, 1098